



## City Research Online

### City, University of London Institutional Repository

---

**Citation:** Gulistan, A., Ghosh, S., Chugh, S. & Rahman, B. M. (2019). Air-holes induced multimodal fiber design to increase the effective index difference between higher order guided modes. *Optical Fiber Technology*, 53, 102023. doi: 10.1016/j.yofte.2019.102023

This is the accepted version of the paper.

This version of the publication may differ from the final published version.

---

**Permanent repository link:** <https://openaccess.city.ac.uk/id/eprint/23010/>

**Link to published version:** <https://doi.org/10.1016/j.yofte.2019.102023>

**Copyright:** City Research Online aims to make research outputs of City, University of London available to a wider audience. Copyright and Moral Rights remain with the author(s) and/or copyright holders. URLs from City Research Online may be freely distributed and linked to.

**Reuse:** Copies of full items can be used for personal research or study, educational, or not-for-profit purposes without prior permission or charge. Provided that the authors, title and full bibliographic details are credited, a hyperlink and/or URL is given for the original metadata page and the content is not changed in any way.

---

---

---

City Research Online:

<http://openaccess.city.ac.uk/>

[publications@city.ac.uk](mailto:publications@city.ac.uk)

---

# Air-holes induced multimodal fiber design to increase the effective index difference between higher order guided modes

Aamir Gulistan<sup>\*1</sup>, Souvik Ghosh<sup>1</sup>, B. M. A Rahman<sup>1</sup>

*School of Mathematics, Computer Science & Engineering (SMCSE), City, University of London, London, EC1V 0HB, U.K*

---

## Abstract

A novel technique is proposed to increase the effective index difference ( $\Delta n_{eff}$ ) between higher order modes of a multimode step-index fiber. Multimode fibers provide a higher effective area and their higher order modes are also resistant to area reduction due to bending. However, the larger effective area comes with an increased number of modes which are more prone to mode coupling and mode mixing. The modal stability is directly related to the effective index difference between the mode of propagation and its neighboring modes. We have shown here that the modal stability between  $LP_{06}$  mode and its neighboring antisymmetric  $LP_{15}$  and  $LP_{16}$  modes can be increased more than 54% by the introduction of air-holes array along the circumference of the fiber. We have also shown variation in the effective index difference with possible fabrication tolerances that may occur in air-holes size and change in their locations. Furthermore, the technique presented here can also be applied to increase the stability of other higher modes of a multimode fiber.

*Keywords:* Multimode fibre, Mode stability, Higher order modes, Effective index difference

---

<sup>\*</sup>Corresponding author

*Email address:* [\\*aamir.gulistan@city.ac.uk](mailto:*aamir.gulistan@city.ac.uk) (Aamir Gulistan\*)

## 1. Introduction

Recently, fiber lasers have received significant attention to generate high optical power with good flexibility and high beam quality [1, 2]. The rapid development of high power pump laser diodes (LD) and use of rare-earth materials in the development of fiber lasers have significantly increased their penetration in different industrial applications [3, 4, 5]. Compared to other types of lasers, the long lengths of fiber lasers make them attractive as they provide large single pass gain for effective power scaling. However, due to the fiber geometry, high intensity light travels under tight confinement for considerably a longer distance that results in increased nonlinear effects [6, 7]. These nonlinear effects such as Self-phase modulation (SPM), Stimulated Brillouin scattering (SBS) and Stimulated Raman scattering (SRS) can destroy the linewidth, spectral and spatial characteristics of fiber laser output emission [8, 9]. Nonlinearity restricts power scaling in conventional Single mode fibers (SMF) due to strong light confinement in a relatively smaller core area [10]. In order to mitigate these nonlinear effects, recent research focus has been to increase the fiber dimensions, such as large mode area (LMA) fibers. Although, this is considered as an efficient way to reduce the nonlinear effects significantly, however, maintaining a high beam quality and achieving a single mode operation becomes difficult with a large core [11]. A single mode operation in LMA fiber can be achieved by lowering the numerical aperture (NA) value but due to fabrication limitations and increased bending loss this value is often restricted to 0.06 [12].

Multimode fibers (MMF) provides a much higher effective area but the existence of many modes may result in the random mode mixing and energy may transfer from a desired mode of propagation to its neighboring modes. The identification and excitation of a selective mode is very important in multimode fibers for lasers and amplifiers related applications. There are different techniques proposed for the efficient excitation of a particular higher order mode, such as the use of self-imaging property of multimode interference, prism-coupling and use of Single mode-Multimode-Multimode fiber structure

etc. [13, 14, 15]. Recently, higher order modes (HOM) of MMF are used for high power fiber lasers as they can provide a more stable single mode operation along with the natural resistance to area reduction due to bending as compared with fundamental mode [16]. Higher order modes of MMF are also more resistant to the mode coupling as the modal stability between HOMs of given a MMF increases with the increase in modal order ( $m$ ). However, external perturbations such as bending field overlap interfaces, or fabrication imperfections can cause energy transfer from a desired higher order  $LP_{0m}$  mode to its neighboring antisymmetric  $LP_{1,m-1}$  and  $LP_{1,m+1}$  modes [17, 18, 19]. Mode coupling strongly depends on the field values [20] at these structural perturbations, but also on the effective index difference between the interacting modes. Here, the modal stability is described by the effective index difference ( $\Delta n_{eff}$ ) between a desired mode of propagation and its neighboring modes, assuming other factors remain similar. The larger fiber dimensions allow fundamental mode along with other higher order modes to propagate with different effective indices ( $n_{eff}$ ). A lower value of  $\Delta n_{eff}$  between the adjacent modes may result in the inter-mode mixing and can cause interference effects. However, increasing the  $\Delta n_{eff}$  between these modes can significantly reduce this inter-mode mixing and any possible interference effects between them.

In this paper, we proposed a novel MMF design to increase the  $\Delta n_{eff}$  between a higher order symmetric mode and its neighboring antisymmetric modes. Ruan *et al* [21] reported different fabrication techniques to generate nanoholes of different sizes in special type optical fibers. Our proposed design uses strategically located small air-hole strip which can be fabricated by adopting a similar approach that is used for the fabrication of Photonic Crystal Fibers (PCF) [21, 22].

For our simulations, we have used a step-index multimode fiber with a core diameter of  $50 \mu m$ . The numerical aperture of the fiber is calculated as  $NA = 0.22$  with the Ge-doped core and pure Silica cladding having refractive indices of  $n_{core} = 1.457$  and  $n_{clad} = 1.4403$ , respectively. The operating wavelength of  $\lambda = 1.05 \mu m$  is considered and COMSOL Multiphysics is used for our simulations.

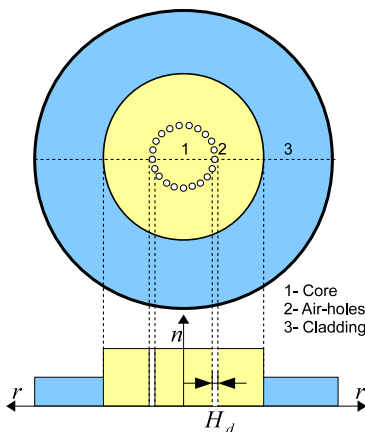


Figure 1: Schematic cross-section design with annular air-holes array and refractive index profile along the radius of a MMF.

For a given MMF, the modal stability between higher order modes increases with the increase in modal order,  $m$ . This means that the  $\Delta n_{eff}$  of a higher order  $LP_{09}$  mode with its neighboring antisymmetric  $LP_{18}$  and  $LP_{19}$  modes have a higher value compared to a lower order mode, say  $LP_{03}$  mode with its adjacent modes. However, exciting a higher order mode may involve more complexity as the power profile of the incident light is required to match the profile of a desired higher order mode to avoid any back reflection. Moreover, for given fiber dimensions the effective area of higher order modes also decreases with the increase in the mode order. So, it may be useful to enhance the modal stability for a specific higher order mode.

Here, for our modal analyses, we have used  $LP_{06}$  mode and aimed to increase the effective index difference between  $LP_{15}$  and  $LP_{16}$  modes. Without any air-holes the effective indices of  $LP_{15}$ ,  $LP_{06}$  and  $LP_{16}$  modes are calculated as 1.4530823, 1.4522882 and 1.4514477, respectively. From these values, the resultant effective index differences  $S_1 = \Delta n_{eff}(LP_{15} - LP_{06})$  and  $S_2 = \Delta n_{eff}(LP_{06} - LP_{16})$  are calculated as 0.000794095 and 0.000840509, respectively.

To increase the  $\Delta n_{eff}$  between  $LP_{06}$  mode and its neighboring antisymmetric  $LP_{15}$  and  $LP_{16}$  modes, a circular array of air-holes is introduced along the

circumference of a MMF. Figure 1 shows the schematic view of the proposed MMF design that includes a circular array of air-holes at a particular distance from the center inside the core of MMF. The refractive index profile along the radius of the MMF is also shown in Fig. 1 where the refractive index of the holes having diameter  $H_d$  is considered as  $n_{hole}=1.0$ .

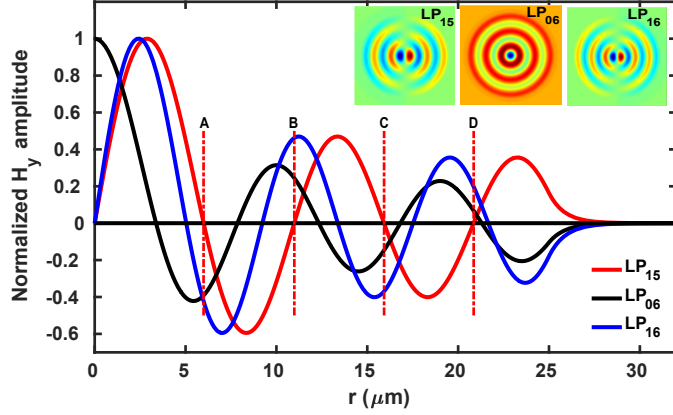


Figure 2: Variations of  $H_y$  fields of the  $LP_{15}$ ,  $LP_{06}$ , and  $LP_{16}$  modes along the r-axis of MMF, contour field profiles in inset and the key points of interest are also shown.

For a given mode, the reduction of its effective index depends on the magnitude of its modal field at the location of air-holes. Figure 2 shows the dominant  $H_y$  field variation of  $LP_{15}$ ,  $LP_{06}$  and  $LP_{16}$  modes along the radius of this MMF. It can be observed that  $LP_{06}$  mode has a maximum amplitude at the center of fiber core ( $r = 0 \mu\text{m}$ ), whereas,  $LP_{15}$  and  $LP_{16}$  modes have zero fields at the center of the fiber core. The contour field profiles of these modes are also shown in Fig. 2 as insets. The zero crossing locations where the field value of these modes is zero are calculated and given in Table 1. Furthermore, zero crossing positions of  $LP_{15}$  mode are also highlighted with letters A, B, C and D in Fig. 2 to assist further discussions.

Table 1: Zero crossing locations of field profiles of the  $LP_{15}$ ,  $LP_{06}$  and  $LP_{16}$  modes along r-axis ( $\mu m$ ).

Mode	Zero crossing locations along r-axis ( $\mu m$ )					
$LP_{15}$	0	5.999	10.985	15.925	20.855	-
$LP_{06}$	3.376	7.855	12.335	16.819	31.305	-
$LP_{16}$	0	5.041	9.225	13.38	17.523	21.66

## 2. Results and Discussion

Technique proposed here include an array of air-holes that decreases the effective indices of  $LP_{06}$  and  $LP_{16}$  modes while keeping the  $LP_{15}$  mode effective index unchanged. Table 2 shows the field values of  $LP_{06}$  and  $LP_{16}$  modes at

Table 2: Normalized field values of  $LP_{06}$  and  $LP_{16}$  modes at the zero crossings A, B, C and D points of  $LP_{15}$  mode.

Optical Modes	A	B	C	D
	5.999	10.985	15.925	20.855
$LP_{06}$	0.3922	0.24435	0.147	0.067695
$LP_{16}$	0.4258	0.46145	0.3693	0.19815
Field values difference ( $LP_{16}-LP_{06}$ )	0.0336	0.2171	0.2223	0.130455

different zero crossing location of the  $LP_{15}$  mode. An air-holes array introduced at the zero crossing locations of  $LP_{15}$  mode would decrease the effective indices of  $LP_{06}$  and  $LP_{16}$  modes, but these decreases will depend on the amplitude of their field values. For example, at the point,  $A = 5.999 \mu m$ , the field value of  $LP_{15}$  mode is zero but the normalized field values of  $LP_{06}$  and  $LP_{16}$  modes are calculated as 0.3922 and 0.4258, respectively, resulting in a field difference of 0.0336. However, at point  $B = 10.985 \mu m$ , the field value difference is calculated as 0.2171, which is higher than the value calculated at Point A. Similarly, at point C the field value difference is calculated as 0.2223. Depending on the

field value difference, the position of air-holes array can be selected to achieve a comparable increase in  $\Delta n_{eff}$  between  $LP_{06}$  and its neighboring  $LP_{15}$  and  $LP_{16}$  modes.

Here, an array of two hundred air-holes at the zero crossing positions A, B, C and D of  $LP_{15}$  mode is introduced with each air-hole diameter taken as  $H_d = 120 \text{ nm}$ . Table 3 shows the absolute change and the percentage change in  $\Delta n_{eff}$  which is calculated with respect to previous value as shown in Eq. 1.

From Table 3, it can be observed that with the introduction of air-holes at A to D positions, the modal stability  $S_1$  has increased. However, unfortunately, a noticeable reduction in the modal stability  $S_2$  is observed because  $\Delta n_{eff}$  between  $LP_{06}$  and  $LP_{16}$  modes reduces when air-holes are introduced at position A.

Table 3: Change in  $\Delta n_{eff}$  with the introduction of air-holes array at the zero crossings of  $LP_{15}$  mode.

$\Delta n_{eff}$	Without holes	A=5.999 $\mu\text{m}$		B=10.985 $\mu\text{m}$		C=15.925 $\mu\text{m}$		D=15.715 $\mu\text{m}$	
		$H_d=120\text{nm}$	%change	$H_d=120\text{nm}$	%change	$H_d=120\text{nm}$	%change	$H_d=120\text{nm}$	%change
$S_1=(LP_{15}-LP_{06})$	0.00079409	0.001874673	136 $\uparrow$	0.001471349	85 $\uparrow$	0.00102064	29 $\uparrow$	0.000843914	6 $\uparrow$
$S_2=(LP_{06}-LP_{16})$	0.00084050	0.000163878	-81 $\downarrow$	0.001003126	19 $\uparrow$	0.001187816	41 $\uparrow$	0.00094461	12 $\uparrow$

$$\% \text{ Change} = \frac{\text{with holes } \Delta n_{eff} - \text{without holes } \Delta n_{eff}}{\text{without holes } \Delta n_{eff}} * 100 \quad (1)$$

This significant reduction around 81% in the  $\Delta n_{eff}$  is due to small field value difference as the reduction in the effective index of  $LP_{06}$  mode is much higher as compared to the  $LP_{16}$  mode. However, at position B, the normalized field value difference between  $LP_{06}$  and  $LP_{16}$  modes is calculated as 0.2171 that resulted in 85% increased in  $S_1$  and also 19% increase in  $S_2$ . Similarly, further away from the core center these modes have reduced field values, however, the normalized field difference at position C is calculated as 0.2223. With the introduction of 200 air-holes array at C position the modal stabilities  $S_1$  and  $S_2$  increase to 29% and 41%, respectively. Similarly, at point D increase in modal stabilities

are calculated as  $S_1 = 6\%$  and  $S_2 = 12\%$ .

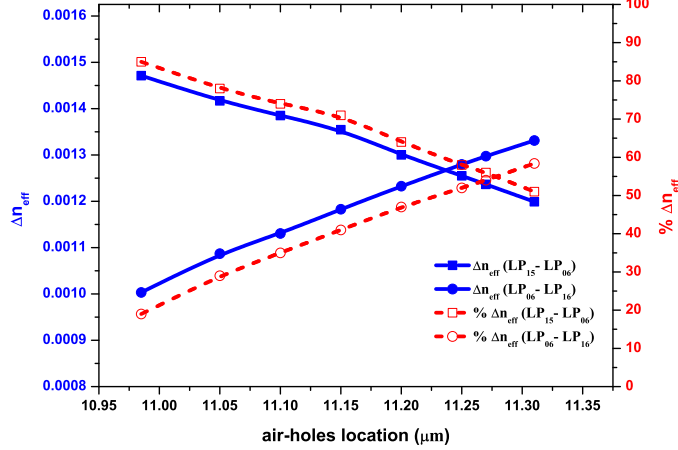


Figure 3: Change in the  $\Delta n_{eff}$  with the location change of air-holes array along the radius of the fiber from point B and fixed 200 air-holes each having diameter of 120 nm.

The  $\Delta n_{eff}$  between the  $LP_{06}$  mode and its neighboring antisymmetric  $LP_{15}$  and  $LP_{16}$  modes has increased significantly with the introduction of air-holes array at B and C positions. However, this increase in effective index difference  $S_1$  and  $S_2$  is not of similar magnitude as in case of position B this was calculated as 85% and 19%, respectively. In order to have a similar or comparable increase in the  $\Delta n_{eff}$ , the position of air-holes array can be adjusted from its original position,  $B = 10.985 \mu m$ . Variation in the  $\Delta n_{eff}$  and the percentage change in the  $\Delta n_{eff}$  is shown in Fig. 3 by solid blue and dashed red lines, respectively, when the air-holes array is shifted from position  $B = 10.985 \mu m$ . As the air-holes array is moved towards the center of the fiber core from position  $B = 10.985 \mu m$ , the modal stability  $S_1$  further increases and  $S_2$  decreases, which may not be desirable. When the air-holes array is shifted 0.085  $\mu m$  towards the core center at 10.9  $\mu m$ , the percentage increase in the modal stabilities  $S_1$  and  $S_2$  are calculated as 99.6% and 0.5%, respectively, but not shown here.

However, when the air-holes array is moved away from the core center towards fiber cladding, the percentage modal stability  $S_1$  starts reducing but  $S_2$  starts increasing. As shown in Fig. 3 the percentage increase in the effective

index difference  $S_1$  and  $S_2$  is nearly equal at position  $B' = 11.27 \mu m$ . At position  $B'$ , the  $\Delta n_{eff}$  between  $LP_{15}$  and  $LP_{06}$  modes is calculated as 0.00123656 and 0.00129738 between  $LP_{06}$  and  $LP_{16}$  modes. The percentage increase in  $S_1$  and  $S_2$  are calculated as 56% and 54%, respectively as shown in Fig. 3 with red dashed lines.

The same trend continues when the air-holes array is shifted further towards the cladding. It should be noted that as the location of air-holes is moved away from the exact zero crossing of the  $LP_{15}$  mode, its effective index will also reduce slightly, but a better control can be achieved in balancing  $S_1$  and  $S_2$ . Hence, for our further analyses, we have used  $B' = 11.27 \mu m$  as the new central position for the air-holes array.

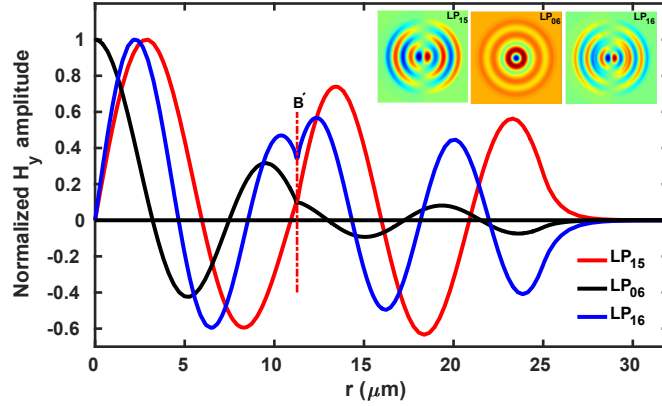


Figure 4: Variations of  $H_y$  fields of the  $LP_{15}$ ,  $LP_{06}$ , and  $LP_{16}$  modes along the r-axis of MMF with the introduction of 200 air-holes array each having  $H_d = 120 nm$ , contour field profiles are also in inset.

Figure 4 shows the variation of  $H_y$  field profiles of  $LP_{15}$ ,  $LP_{06}$  and  $LP_{16}$  modes along the radius of the MMF after the introduction of air-holes. Here, 200 hundred air-holes having  $H_d = 120 nm$  are introduced at  $B'$  position along the circumference of MMF. Following the introduction of air-holes, the effective indices of  $LP_{15}$ ,  $LP_{06}$  and  $LP_{16}$  modes are reduced and new values are calculated as 1.45303814, 1.451801579 and 1.45050419, respectively. Moreover, the normalized field values at position  $B'$  after the introduction of air-holes also

reduced and these new values are calculated as 0.107, 0.098 and 0.3427 for the  $LP_{15}$ ,  $LP_{06}$  and  $LP_{16}$  modes, respectively. From the  $H_y$  field variations of these modes shown in Fig. 4, it can be observed that the field profiles modify after the  $B'$  position due to the presence of these air-holes. The contour plots of  $LP_{15}$ ,  $LP_{06}$  and  $LP_{16}$  modes after the introduction of air-holes are also shown in Fig. 4 as insets.

### 3. Fabrication tolerance

The drill-and-draw or extrusion technique can be used for the fabrication of such micro-structured fibers consisting of air-holes [23]. However, with the smaller air-holes, the fabrication process can become more challenging as due to drilling in the preform or during the drawing process, air-holes diameter or their position can slightly change.

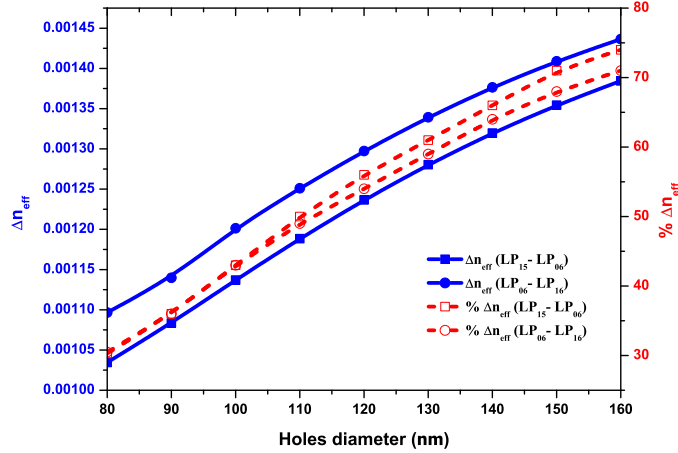


Figure 5: Change in the absolute and percentage effective index difference  $S_1$  and  $S_2$  with the variation in the holes diameter with fixed 200 hundred holes.

In order to observe variation in the  $\Delta n_{eff}$  due to change in the air-holes diameter (from 120 nm) or in their position, further numerical simulations were carried out. Figure 5 shows the change in the effective index differences  $S_1$  and  $S_2$  with the change in the diameter of air-holes introduced at  $B'$  radial position.

It can be observed that with the reduction in the air-holes diameter from 120 nm to a lower value, the effective index difference  $S_1$  and  $S_2$  also decrease linearly. When 200 air-holes having a diameter of 80 nm are introduced at the  $B'$  position, the percentage increase in the effective index difference decreased and calculated as  $S_1 = 30.3\%$  and  $S_2 = 30.5\%$ . The respective absolute  $\Delta n_{eff}$  values are also shown by blue lines in Fig. 5. However, when the air-holes diameter is increased to more than 120 nm, the percentage increase in the  $\Delta n_{eff}$  also increases and for a diameter of 160 nm the percentage increase in the effective index difference is calculated as  $S_1 = 74\%$  and  $S_2 = 71\%$ . The above analysis also shows that even with the change of  $\pm 40$  nm in air-holes diameter, the percentage increase in modal stability still remains above 30%.

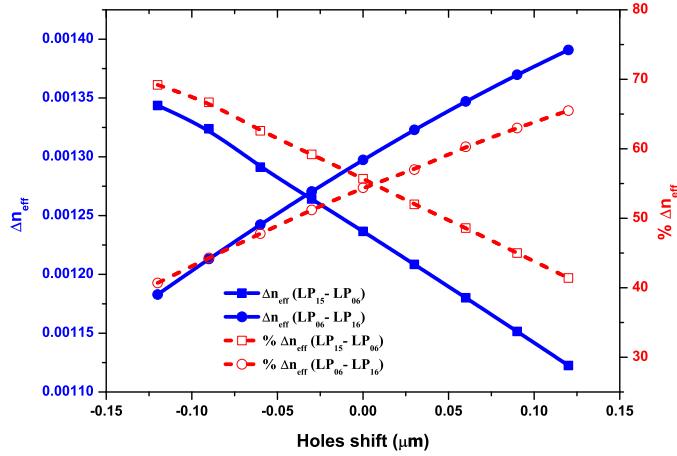


Figure 6: Change in the real and percentage effective index difference  $S_1$  and  $S_2$  with the shift of air-holes array from central location  $R_{loc}=11.27 \mu m$ .

One of the fabrication related issues may arise if the air-holes array is shifted from its central position, as for the above case, from  $B' = 11.27 \mu m$ . Figure 6 shows the change in the  $\Delta n_{eff}$  and percentage  $\Delta n_{eff}$  with the shift in the air-holes array position. When 200 air-holes having  $H_d = 120$  nm are introduced at  $11.15 \mu m$  (shift of  $-0.12 \mu m$  from  $B'$  position) the effective index difference  $S_1$  and  $S_2$  are calculated as  $0.001343699$  and  $0.001182876$ , respectively yielding the percentage as  $69.2\%$  and  $40.7\%$  for  $S_1$  and  $S_2$ , respectively. Similarly, when

the air-holes array is shifted to  $11.39 \mu m$  position which is  $+ 0.12 \mu m$  shift from  $B'$  position, the resultant effective index differences of  $S_1$  and  $S_2$  are calculated as 0.001122553 and 0.001390885, respectively. Here, it should be noted that the percentage improvement in  $\Delta n_{eff}$  remains above 40% even with the shift of  $\pm 0.12 \mu m$  from the central  $B'$  position.

In Fig. 5, it is shown that the percentage  $\Delta n_{eff}$  was increased up to 56% with 200 air-holes having 120 nm air-holes diameter. However, considering  $B'$  a central position for air-holes, we carried out further simulations to achieve similar effective index difference with less number of air-holes, which may be easier to fabricate.

Table 4: Multiple combinations of air-holes diameter and quantity to achieve similar increase in effective index difference.

$\Delta n_{eff}$	Without air-holes	200 air-holes array		100 air-holes array		50 air-holes array	
		$H_d=120nm$	% Increase	$H_d=176nm$	% Increase	$H_d=286nm$	% Increase
$S_1=LP_{15} - LP_{05}$	0.000794095	0.00123656	56	0.001246015	57	0.001243745	57
$S_2=LP_{05} - LP_{16}$	0.000840509	0.001297389	54	0.001286119	53	0.001287225	53

Table 4 summarizes different combinations of air-holes size and resulting increase in the  $\Delta n_{eff}$  between  $LP_{15}$ ,  $LP_{06}$  and  $LP_{16}$  modes. When 100 air-holes with 176 nm diameter are introduced at  $B'$  position the resultant percentage increase in  $S_1 = 57\%$  and  $S_2 = 53\%$  are nearly equal to the initially proposed design with 200 air-holes having  $H_d = 120$  nm. Similarly, when the number of air-holes is further reduced to 50 and air-holes diameter increased to  $H_d = 286$  nm, the respective percentage increase in  $\Delta n_{eff}$  is calculated as  $S_1 = 57\%$  and  $S_2 = 53\%$ . Moreover, the number of air-holes can be further reduced along with the increased  $H_d$  (e.g. 25 air-holes having diameter  $H_d = 580$  nm) to achieve a similar increase in the  $\Delta n_{eff}$ . This shows that the proposed technique is flexible in terms of the number of air-holes and also their dimensions that can be useful for a specific fabrication technique considered.

#### 4. Scalability of Proposed Technique

Furthermore, we have used similar approach to enhance the effective index difference between  $LP_{08}$  mode and its neighboring antisymmetric  $LP_{17}$  and  $LP_{18}$  modes. Figure 7 shows the  $H_y$  field variation of  $LP_{17}$ ,  $LP_{08}$  and  $LP_{18}$  modes along the radius of the MMF. The contour field profiles of these modes are also

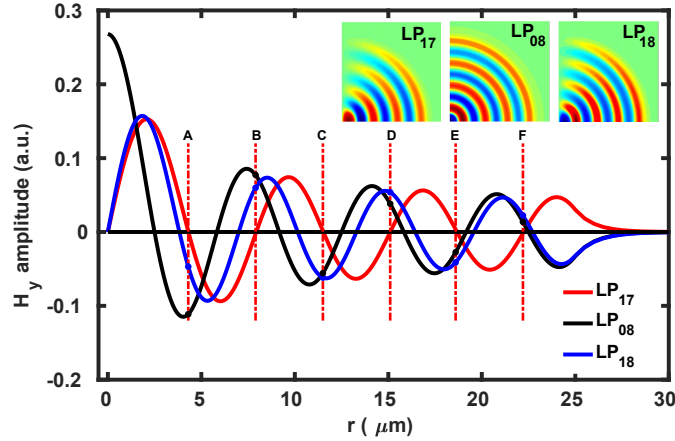


Figure 7: Variations of  $H_y$  fields of the  $LP_{17}$ ,  $LP_{08}$ , and  $LP_{18}$  modes along the r-axis of MMF, contour field profiles in inset and the key points of interest are also shown.

shows in Fig. 7 as insets. Unlike  $LP_{15}$  mode, the  $LP_{17}$  mode has more zero crossing locations labeled as positions A to F in Fig. 7. These zero crossing positions of  $LP_{17}$ ,  $LP_{08}$  and  $LP_{18}$  modes are also given in Table 5. The effective indices of  $LP_{17}$  and  $LP_{08}$  and  $LP_{18}$  modes are calculated as 1.4495339, 1.4484630 and 1.4473461, respectively.

Without introduction of air-holes, the modal stabilities  $S'_1 = \Delta n_{eff}(LP_{17} - LP_{08})$  and  $S'_2 = \Delta n_{eff}(LP_{08} - LP_{18})$  between these modes are calculated as 0.001070831 and 0.001116877, respectively. As discussed in the introduction that the modal stability increases with the increase in the modal order ( $m$ ), hence the original  $\Delta n_{eff}$  values for  $LP_{08}$  mode is higher than that of the  $LP_{06}$  mode.

Using the similar approach as discussed earlier, an array of 200 air-holes

Table 5: Zero crossing locations of field profiles of the  $LP_{17}$ ,  $LP_{08}$  and  $LP_{18}$  modes along  $r$ -axis ( $\mu\text{m}$ ).

Mode	Location of zero crossings along r-axis ( $\mu\text{m}$ )						
$LP_{17}$	0	4.30	7.90	11.50	15.10	18.60	22.20
$LP_{08}$	2.40	5.80	9.10	12.40	15.80	19.10	22.40
$LP_{18}$	0	3.80	7.00	10.10	13.20	16.40	19.50

with diameter  $H_d = 120 \text{ nm}$  are introduced at the zero crossing locations of  $LP_{17}$  mode and the resultant increase in the modal stabilities  $S'_1$  and  $S'_2$  are calculated. The effective index differences due to air-holes at point  $D = 15.10 \mu\text{m}$  are calculated as  $S'_1 = 0.00137816$  and  $S'_2 = 0.00154139$  which represents 29% and 38% increase in the percentage modal stabilities, respectively.

For an identical increase in the percentage modal stabilities  $S'_1$  and  $S'_2$ , the location of air-holes array is adjusted from  $D = 15.10$  to  $D' = 15.0$ . The resultant increase in the modal stabilities with the combination of different air-holes size and quantity are given in Table 6. The percentage increase in the modal stability of  $S'_1 = 34\%$  and  $S'_2 = 36\%$  is achieved with the 200 air-holes having  $H_d = 120 \text{ nm}$ . A similar percentage increase is calculated when 100 air-holes having  $H_d = 180 \text{ nm}$  and 50 air-holes having  $H_d = 300 \text{ nm}$  are introduced at the position  $D'$  along the radius of MMF, as given in Table 6. This shows that the proposed technique is scalable and can be used for a given higher order mode as required and its neighboring modes in a MMF. Moreover, a different combination of air-holes numbers and their size can also be chosen to achieve a similar increase in the  $\Delta n_{eff}$ .

## 5. Conclusions

A novel approach is proposed to increase the modal stability of higher order modes in a multimode fiber using air-holes. Multimode fibers provide higher effective area along with the increased modal stability in higher order modes.

Table 6: Different combinations of air-holes diameter and quantity to increase the  $\Delta n_{eff}$  between  $LP_{08}$  mode and its neighboring antisymmetric  $LP_{17}$  and  $LP_{18}$  modes.

$\Delta n_{eff}$	Without air-holes	200 air-holes array		100 air-holes array		50 air-holes array	
		$H_d=120nm$	% Increase	$H_d=180nm$	% Increase	$H_d=300nm$	% Increase
$S_1=LP_{17} - LP_{08}$	0.001070831	0.001437158	34	0.001437728	34	0.00143702	34
$S_2=LP_{08} - LP_{18}$	0.001116877	0.001515669	36	0.00151080	35	0.001504782	35

We have shown that the effective index difference  $\Delta n_{eff}$  between  $LP_{06}$  mode and its neighboring antisymmetric  $LP_{15}$  and  $LP_{16}$  modes can be increased more than 54% by introducing air-holes along the circumference of multimode fiber. The increased modal stability reduces the modal cross talk and interference between HOMs of MMF and may result in a better performance for fiber lasers. The proposed technique is also scalable and we have shown that the percentage  $\Delta n_{eff}$  between  $LP_{08}$  mode and its neighboring  $LP_{17}$  and  $LP_{18}$  modes can also be increased to more than 34% by using the proposed method. Moreover, it was noted that with the introduction of air-holes the effective area also slightly reduces, but the improvement in the modal stability has increased significantly.

## References

- [1] M. N. Zervas and C. A. Codemard, High power fiber lasers: a review, IEEE J. Sel. Top. Quantum Electron 20 (5) (2014) 219–241 .
- [2] C. Jauregui, J. Limpert, and A. Tunnermann, High-power fibre lasers, Nat. Photonics 7 (11) (2013) 861.
- [3] E. Zucker, D. Zou, L. Zavala, H. Yu, P. Yalamanchili, L. Xu, H. Xu, D. Venables, J. Skidmore, V. Rossin, and R. Raju, Advancements in laser diode chip and packaging technologies for application in kW-class fiber laser pumping, High-Power Diode Laser Technology and Applications XII 8965 (2014).

- [4] S. Fu, W. Shi, Y. Feng, L. Zhang, Z. Yang, S. Xu, X. Zhu, R. A. Norwood, and N. Peyghambarian, Review of recent progress on single-frequency fiber lasers, *J. Opt. Soc. Am. B* 34 (3) (2017) A49–A62.
- [5] I. Savellii, L. Bigot, B. Capoen, C. Gonnet, C. Chaneac, E. Burova, A. Pastouret, H. El-Hamzaoui, and M. Bouazaoui, Benefit of Rare-Earth “Smart Doping” and Material Nanostructuring for the Next Generation of Er-Doped Fibers, *Nanoscale Res. Lett.* 12 (1) (2017) 206.
- [6] W. S. Wong, X. Peng, J. M. McLaughlin, and L. Dong, Breaking the limit of maximum effective area for robust single-mode propagation in optical fibers, *Opt. Lett.* 30 (21) (2005) 2855–2857.
- [7] J. Limpert et al., High Repetition Rate Gigawatt Peak Power Fiber Laser Systems: Challenges, Design, and Experiment, *IEEE J. Sel. Top. Quantum Electron* 15 (1) (2009) 159–169.
- [8] J. Limpert, F. Stutzki, F. Jansen, H. J. Otto, T. Eidam, C. Jauregui, and A. Tunnermann, Yb-doped large-pitch fibres: effective single-mode operation based on higher-order mode delocalisation, *Light Sci. Appl.* 1 (4) (2012) e8.
- [9] D. J. Richardson, J. Nilsson, and W. A. Clarkson, High-power fiber lasers: current status and future perspectives, *J. Opt. Soc. Am. B* 27 (11) (2010) B63–B92.
- [10] A. Tunnermann, T. Schreiber and J. Limpert, Fiber lasers and amplifiers: an ultrafast performance evolution, *Appl. Opt.* 49 (25) (2010) F71–F78.
- [11] F. Stutzki, F. Jansen, H. J. Otto, C. Jauregui, J. Limpert, and A. Tunnermann, Designing advanced very-large-mode-area fibers for power scaling of fiber-laser systems, *Optica* 1 (4) (2014) 233–242.
- [12] F. Kong, C. Dunn, J. Parsons, M. T. Kalichevsky-Dong, T. W. Hawkins, M. Jones, and L. Dong, Large-mode-area fibers operating near single-mode regime, *Opt. Express* 24 (10) (2016) 10295–10301.

- [13] X. Zhu, A. Schulzgen, H. Li, L. Li, Q. Wang, S. Suzuki, V. L. Temyanko, J. V. Moloney, and N. Peyghambarian, Single-transverse-mode output from a fiber laser based on multimode interference *Opt. Lett.* 33 (9) (2008) 908–910.
- [14] B. M. Trabold, D. Novoa, A. Abdolvand, and P. St. J. Russell, Selective excitation of higher order modes in hollow-core PCF via prism-coupling, *Opt. Lett.* 39 (13) (2014) 3736–3739.
- [15] N. Bhatia, K. C. Rustagi, and J. John, Single  $LP_{0,n}$  mode excitation in multimode fibers, *Opt. Express* 22 (14) (2014) 16847–16862.
- [16] J. M. Fini and S. Ramachandran, Natural bend-distortion immunity of higher-order-mode large-mode-area fibers, *Opt. Lett.* 32 (7) (2007) 748–750.
- [17] S. Ramachandran, J. W. Nicholson, S. Ghalmi, M. F. Yan, P. Wisk, E. Monberg, and F. V. Dimarcello, Light propagation with ultralarge modal areas in optical fibers, *Opt. Lett.* 31 (12) (2006) 1797–1799.
- [18] S. Ramachandran, J. M. Fini, M. Mermelstein, J. W. Nicholson, S. Ghalmi, and M. F. Yan, Ultra-large effective-area, higher-order mode fibers: a new strategy for high-power lasers, *Laser Photonics Rev.* 2 (6) (2008) 429–448.
- [19] A. Gulistan, S. Ghosh, S. Ramachandran, and B.M.A. Rahman, Efficient strategy to increase higher order inter-modal stability of a step index multimode fiber, *Opt. Express* 25 (24) (2017) 29714–29723.
- [20] E. N. Fokoua, N. Wong, D. J. Richardson, and F. Poletti, Analysis and comparison of intermodal coupling coefficient of standard and hollow core few moded fibres, In *Optical Communication (ECOC), 2015 European Conference on*, (2015) 1-3.
- [21] Y. Ruan, H. Ebendorff-Heidepriem, S. Afshar, and T. M. Monro, Light confinement within nanoholes in nanostructured optical fibers, *Opt. Express* 18 (25) (2010) 26018–26026.

- [22] C. M. Rollinson, S. T. Huntington, B. C. Gibson, S. Rubanov, and J. Canning, Characterization of nanoscale features in tapered fractal and photonic crystal fibers, *Opt. Express* 19 (3), (2011) 1860–1865.
- [23] R. S. Windeler, Microstructure Fibers, *Encyclopedia of Modern Optics*, Academic Press 195 (2018).